EAN 2017
55th conference on experimental stress analysis

Effects of Advanced Laser Processing on the Microstructure and Residual Stresses of H13 Tool Steel

Karel Trojan[1,a], Václav Ocelík[2,b], Nikolaj Ganev[1,c], Stanislav Němeček[3,d] and Jiří Čapek[1,e]

[1]CTU in Prague, Department of Solid State Engineering, Faculty of Nuclear Sciences and Physical Engineering, Trojanova 13, 120 00 Prague 2, Czech Republic

[2]Department of Applied Physics, Zernike Institute for Advanced Materials, Faculty of Science and Engineering, University of Groningen, Nijenborgh 4, 9747 AG, Groningen, The Netherlands

[3]RAPTECH s. r. o. ,U Vodárny 473, 330 08 Zruč-Senec, Czech Republic

[a]karel.trojan@fjfi.cvut.cz, [b]v.ocelik@rug.nl, [c]nikolaj.ganev@fjfi.cvut.cz, [d]nemecek@raptech.cz [e]jiri.capek@fjfi.cvut.cz

Keywords: laser processing; cladding; residual stresses; microstructure; H13 tool steel.

Abstract. The aim of this paper is to describe the effects of laser processing on the microstructure and residual stresses of laser cladded H13 tool steel on the classical construct steel S355 substrate. This research paper concludes that in this case of laser cladding, phase transformation and not shrinkage is likely to be a dominant effect on the formation of compressive residual stresses along the clad. Furthermore, martensitic structure and unequal concentration of alloying elements was observed on the cross-section of the clad using electron backscattering diffraction and energy-dispersive X-ray spectroscopy.

Introduction

Processing by high power lasers is nowadays the standard in many different industrial fields which require precision, accuracy and high production efficiency. Therefore, this paper outlines the capability of the advanced laser processing for additive manufacturing in relation to Telesang et al. (2015) [1]. Hot working tool steel H13 is one of the most common die material used in metal and casting industries. Dies suffer great damage due to wear and thermo-dynamic stresses during their lifetime [1]. Therefore, various methods have been developed for its repair. A great benefit of laser cladding in this field is a high productivity along with minimal influence on surrounding material by thermal stress [2]. This study reports an investigation of residual stresses (RS) by X-ray diffraction (XRD) and microstructure (chemical and phase composition, crystallite orientation) by orientation imaging microscopy (OIM) using electron backscatter diffraction (EBSD) and energy-dispersive X-ray spectroscopy (EDS) with scanning electron microscopy (SEM) of laser cladded tool steel AISI H13 on the classical construct steel S355 substrate. The research aims to understand the residual stresses and microstructural characteristics that are one of the most important factors that influence the products behaviour, especially the fatigue life [3].

Experimental

Laser cladding was carried using a diode laser *Laserline* 5,5kW with optical head *Precitec Y52*. Laser power density 108 J/mm^2 was applied to form a single clad with the length of 137 mm, width of 6 mm and height of approx. 1 mm above substrate. The powder of the AISI H13 tool steel was used with an average particles diameter of 53.1 ± 15.9 μm.

X-ray diffraction analysis was carried out using an *X´Pert PRO MPD* diffractometer with chromium tube anode and pinholes determining irradiated area of primary beam, with size of 1×0.5 mm^2 in longitudinal clad direction L and 2×0.25 mm^2 in transversal clad direction T, respectively. Diffraction angle $2\theta^{211}$ was taken as a centre of gravity of the {*211*} diffraction doublet *CrKα*. For residual stress evaluation, $\sin^2\psi$ method and X-ray elastic constants $½s_2$ = 5.76 TPa^{-1} and s_1 = –1.25 TPa^{-1} were used.

In order to determine the phase composition of the surface layer, diffraction patterns were obtained by measuring the clad on the instrument *X'Pert PRO MPD* in classical Bragg – Brentano (BB) focusing configuration with cobalt tube anode and 1×0.25 mm^2 pinholes. Measured diffraction diagrams were processed with the program *X'Pert HighScorePlus* and crystalline phases were identified using a *PDF-2* database. Quantitative analysis was evaluated using the Rietveld analysis in the *TOPAS 4.2* software. The effective depth of penetration (T^{eff}) is corresponding to the thickness of a surface layer that provides about 63 % of the diffracted intensity. In the case of the used wavelength, the T^{eff} is about 5 μm.

The OIM data was collected using a *Philips XL 30 FEG* scanning electron microscope equipped with a *TSL OIM system* based on *DigiView 3* camera and *EDS EDAX SUTW+* detector. The accelerating voltage of 25 kV and 0.4 μm step size of scanning were used. A grain boundary is defined in the microstructure as a boundary between two neighbouring scanning points having crystallographic misorientation larger than 5°. All EBSD data were analysed with *TSL OIM Analysis 7.3.0* software and only data points with *Confident index* higher than 0.05 were used. *Confident index* is based on voting scheme during automated indexing of the diffraction pattern where it is counted as a ratio of votes for the best solution minus votes for the second best solution divided by total possible number of votes from the detected Kikuchi bands. Certain crystallographic orientation receives a vote when observed angles between the three bands are the same as table values of given orientation. *Confident index* 0.05 corresponds on a face-centred cubic material to approx. 70% probability of correct indexing.

Results and discussion

Table 1 gives the range of the chemical composition of H13 steel determined quoted by ISO 4957 [4], the next row shows average chemical composition and standard deviation obtained by EDS on a cross-section of four randomly selected particles of the used powder obtained by EDS on a cross-section; the bottom row shows the average chemical composition and standard deviation in four different clad cross-section areas of dimensions approx. 500×250 μm^2. Table 1 shows that only chromium in the clad is on average about one weight percentage less than prescribe standard. Manganese has been observed on the contrary of 0.1 % or more. SEM image of the cross-section of the single clad with used directions and an area 200×200 μm^2 which was observed using OIM can be seen in Fig. 1. Lack of the fusion on the sides of the clad could be observed, it is probably the result of improper setting of laser power density.

Table 1: Chemical composition of the steel AISI H13 according ISO 4957 [4], the powder AISI H13 and the clad.

	Cr [Wt.%]	Mo [Wt.%]	Si [Wt.%]	V [Wt.%]	Mn [Wt.%]	C [Wt.%]
EN ISO 4957	4.80 – 5.50	1.20 – 1.50	0.80 – 1.20	0.85 – 1.15	0.25 – 0.50	0.35 – 0.42
Powder H13	5.10 ± 0.07	1.79 ± 0.08	0.92 ± 0.11	1.08 ± 0.02	0.45 ± 0.07	
Clad	3.77 ± 0.05	1.21 ± 0.05	0.72 ± 0.01	0.84 ± 0.03	0.62 ± 0.03	

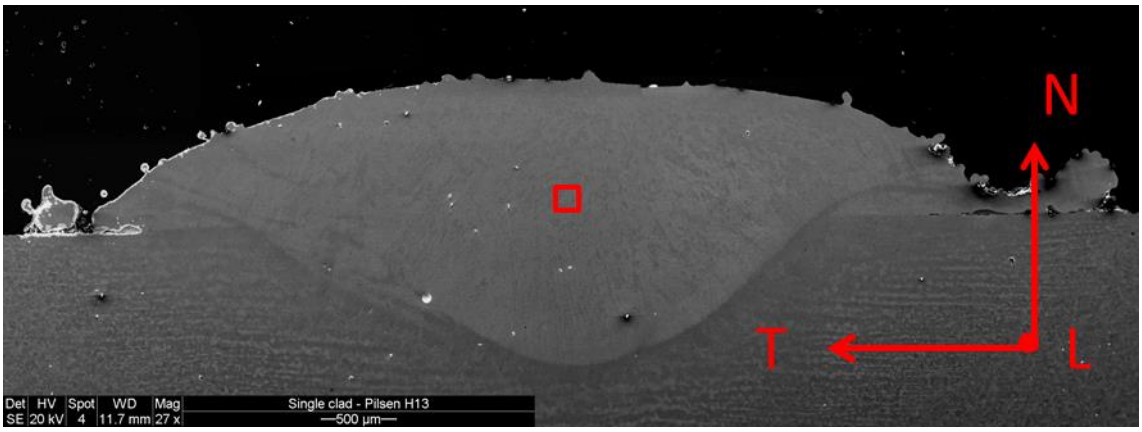

Fig. 1: SEM image of the cross-section of the single clad AISI H13 tool steel with marked directions and area which was observed using OIM.

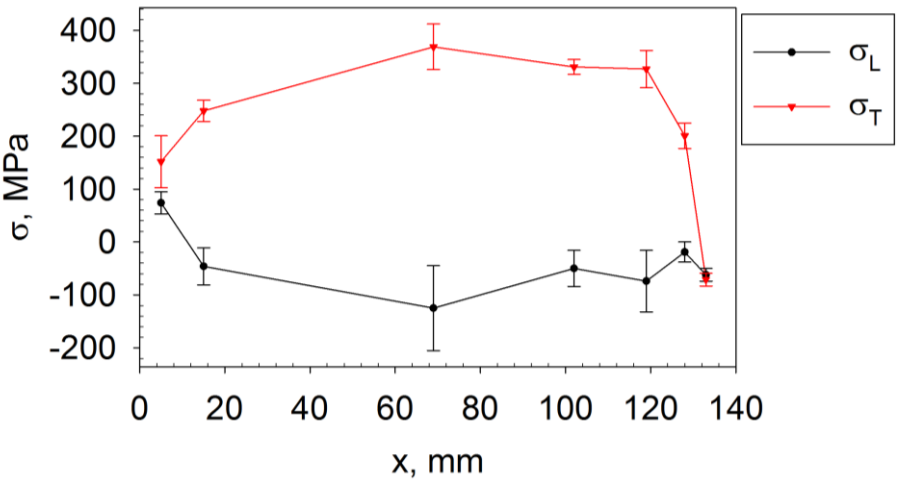

Fig. 2: Surface RS on the top of the clad in direction L and T along the length of laser track, where *x* is the distance from the beginning of the clad.

The comparison of surface RS obtained by XRD in direction L and T is plotted in Fig. 2. RS at the beginning and the end of the clad are comparable with the experimental error. In the direction L, RS exhibit slight compressive stresses along the clad. However, in the direction T, tensile RS were obtained. This dependence is opposite to what was generally observed in the literature [1,5]. However, there were published studies confirming tensile residual stresses in the transversal direction as well [6].

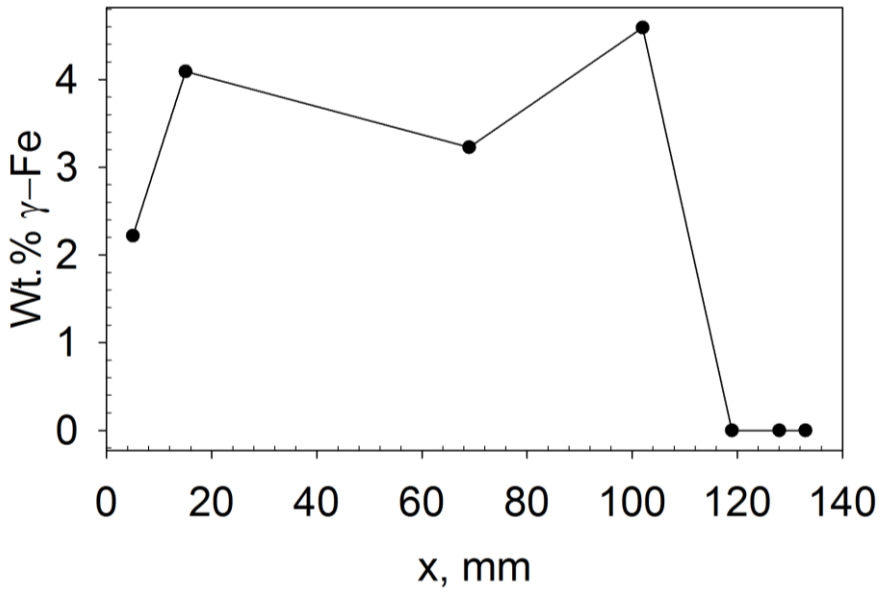

Fig. 3: Mass weight content of γ-Fe in the surface layer obtained by XRD.

Mass weight content of γ-Fe in the surface layer depending on the distance from the beginning of the clad is plotted in Fig. 3. It can be seen that at the beginning of the clad a γ-Fe content is increasing to the value of around 4 %, and in the end no retained austenite was observed by XRD. This could be due to slower cooling rate at the end as the heating of the substrate occurred. After finding these results, the real structure and the microstructure of the single clad have been taken to deeper evaluation by OIM on the cross-section 5 mm from the beginning of the clad.

The main phase detected in the clad was body centred-cubic iron. Fig. 4 shows inverse pole figure maps of α-Fe in the selected area, wherein individual colours correspond to the normal vectors of crystallographic planes that are parallel to the given sample direction. The original austenite grains with a characteristic size of 20-50 μm, which were established during the transition of the melt into a solid phase and whose were subsequently transformed into martensitic laths are clearly seen in the figure. It has to be noted that EBSD technique is not able directly distinguish ferrite and martensite. Carbides of alloying elements were not observed using EBSD. However, in the analysed area, 1.1 % of retained austenite was confirmed. The difference compared to the XRD value could be caused by an error of each method and by larger volumes analysed by XRD, especially along the clad. At the beginning of the clad, proportion of retained austenite by XRD is growing.

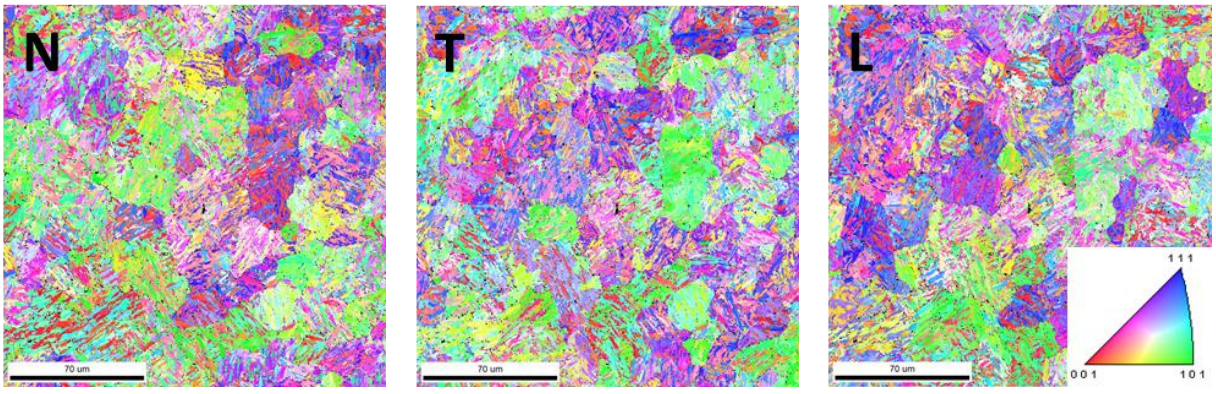

Fig. 4: Orientation maps of α-Fe for different directions in the selected area.

Fig. 5 gives an idea of the relative distribution of individual alloying elements in the selected area obtained by energy-dispersive X-ray spectroscopy mapping. Darker colours indicate higher concentration of the element.

Subsequently, the distribution of the misorientation angle in the selected area is plotted in Fig. 6. In the article [7], there was shown that misorientation angles between the variants that satisfy the Kurdjumov-Sachs orientation relationship of phase transformation from face-centred cubic phase to body-centred cubic phase are up to 21.06° and then higher than 47.11°.

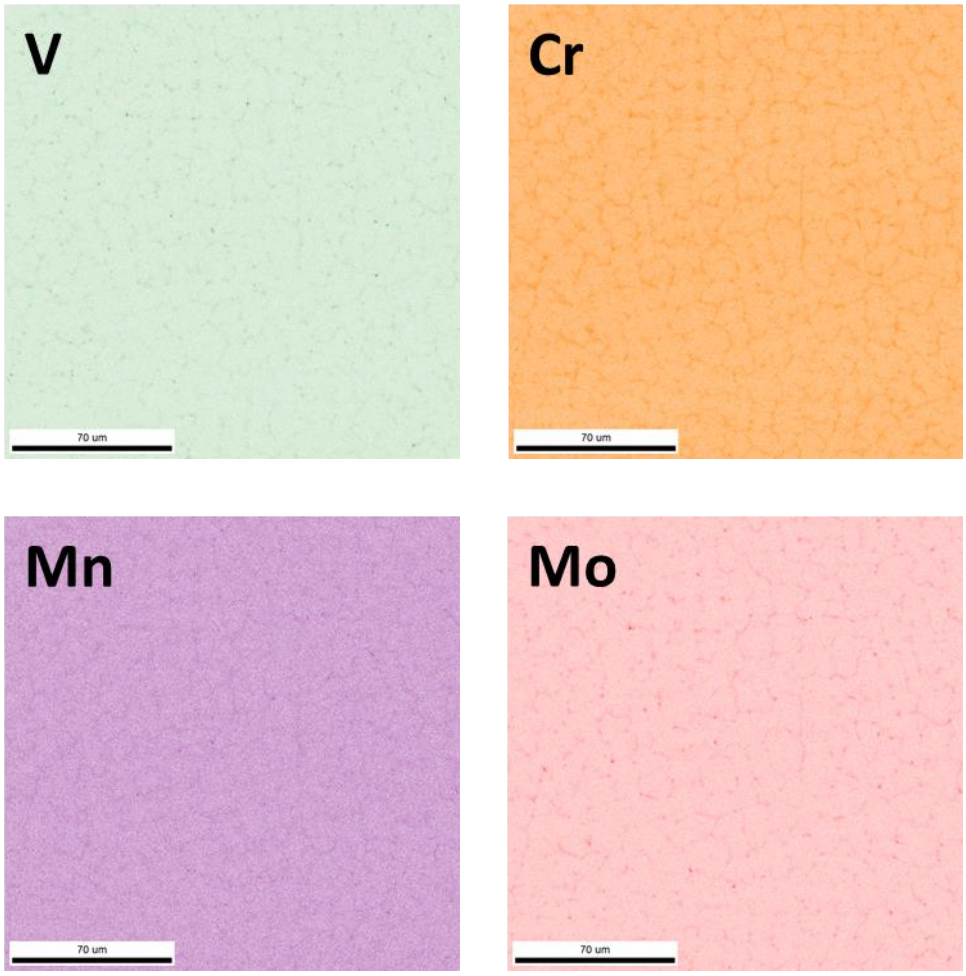

Fig. 5: Relative representation of content of alloying elements in the selected area acquired by EDS.

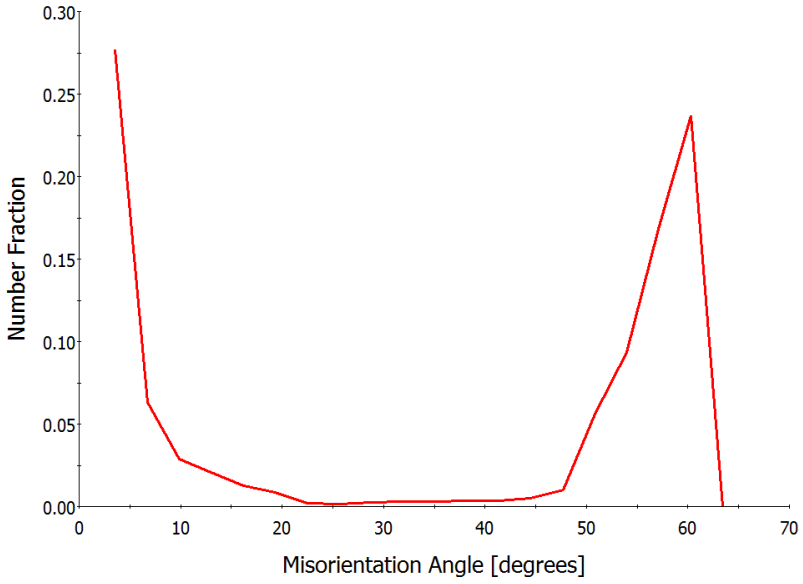

Fig. 6: Misorientation angle distribution in the selected area.

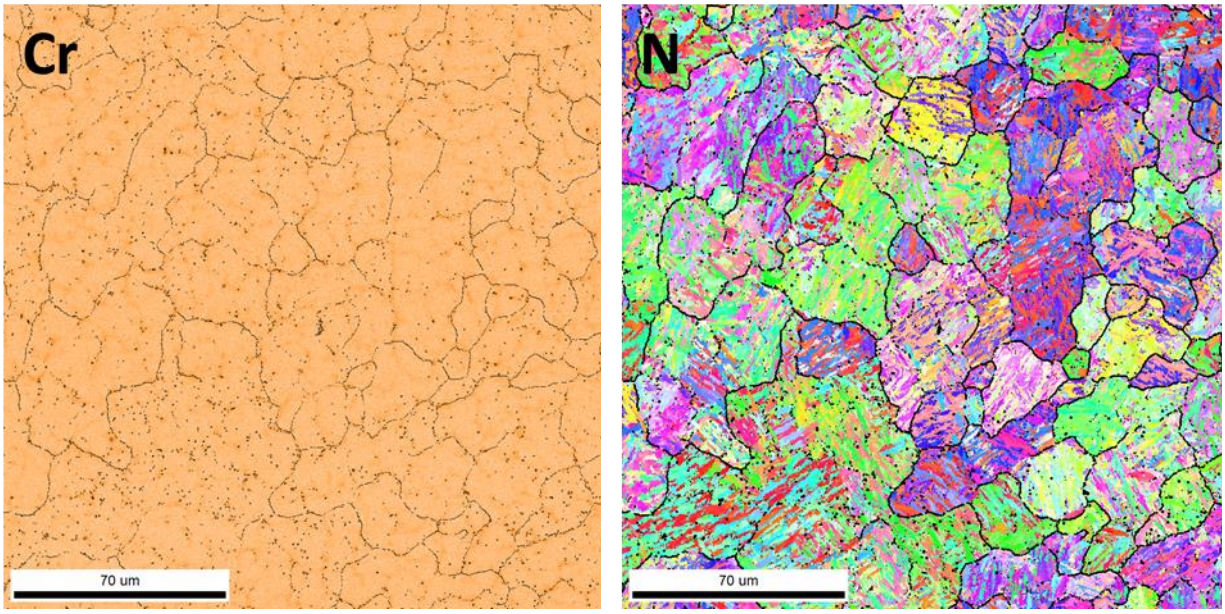

Fig. 7: Comparison of the map of relative representation of content of chromium and orientation map with highlighted grain boundaries between 21.2° and 47°.

Thus, Fig. 7 compares the map of relative representation of content of chromium and grain orientation map with highlighted grain boundaries between 21.2° and 47°. It can therefore be clearly seen that higher concentration of chromium corresponds with the random grains boundaries between 21.2° and 47°. These boundaries relate to the grain boundaries of the original austenitic grains which were formed during cooling of the melt. The unequal concentration of alloying elements is caused by the lever rule during solidification. This could induce inferior mechanical properties of the steel as carbides of alloying elements were not observed.

According to the linear equation developed by Andrews [8], M_s temperature is 316 °C for the lower limit of alloying elements and 268 °C for upper limit of alloying elements [9]. So if we assume that the coefficient of thermal expansion for steel H13 is 12.5×10^{-6} K^{-1}, relative shrinkage 0.0034 results from cooling from the average M_s to the room temperature [10]. On

the other hand, the volume changes during phase transformation in steels are a function of carbon content. Dimensional change during transformation from spheroidite to martensitic microstructure is 0.0026×(Wt.% of C) [9]. For steel H13, the dimensional change is therefore between 0.0020 and 0.0024. Shrinkage and expansion are therefore the same order of magnitude and depends on the specific situation that prevails. Consequently, it depends on the particular situation which effect would be dominant.

The results above suggest that there has been a rapid cooling of the melt to form a martensitic structure. Moreover, no carbides and a half of the value of retained austenite in comparison with XRD were observed using EBSD. Therefore, it may be concluded that in this case of laser cladding, phase transformation and not shrinkage is likely to be a dominant effect on the formation of residual stress in the direction L along the clad. This caused the tensile RS in the perpendicular direction T.

Conclusions

Laser deposition of the H13 tool steel showed a great application potential. Martensitic structure dominates in the single clad. This suggests high cooling rates and quenching of the clad. Laser deposition of H13 induced significant residual stresses. Residual stresses at the beginning and at the end of the track are almost equal within the error. In the longitudinal direction RS exhibit slight compressive character along the clad. However, in the transversal direction tensile RS were detected. The research topic and primarily the main origin of residual stresses has not yet been accurately described and understood, so further measurements and adjustments of the deposition parameters will be needed.

Acknowledgement

Measurements were supported by the project TH02010664 of the Technology Agency of the Czech Republic and by University of Groningen. This work was supported by the Student Grant Competition CTU in Prague grant No. SGS16/245/OHK4/3T/14.

References

[1] G. Telasang, J. Majumdar, N. Wasekar, G. Padmanabham, I. Manna, Microstructure and Mechanical Properties of Laser Clad and Post-cladding Tempered AISI H13 Tool Steel. Metall. Mater. Trans. A. 46A (2015) 2309-2321.

[2] M. Vedani, B. Previtali, G.M. Vimercati, A. Sanvito, G. Somaschini, Problems in laser repair-welding a surface-treated tool steel, Surf. Coat. Tech. 201 (2007) 4518-4525.

[3] G.E. Totten, M. Howes, T. Inoue, Handbook of residual stress and deformation of steel, ASM International, Materials Park, 2002.

[4] ISO 4957:1999. Tool steels.

[5] J. Chen, S. Wang, L. Xue, On the development of microstructures and residual stresses during laser cladding and post-heat treatments, J. Mater. Sci. 47.2 (2012) 779-792.

[6] A. Suárez, J.M. Amado, M.J. Tobar, A. Yáñez, E. Fraga, M.J. Peel, Study of residual stresses generated inside laser cladded plates using FEM and diffraction of synchrotron radiation, Surf. Coat. Tech. 204 (2010) 1983-1988.

[7] H. Kitahara, R. Ueji, N. Tsuji, Y. Minamino, Crystallographic features of lath martensite in low-carbon steel, Acta. Mater. 54 (2006) 1279-1288.

[8] K.W. Andrews, Empirical Formulae for the Calculation of Some Transformation Temperatures, Journal of the Iron and Steel Institute 203 (1965) 721–727.

[9] G. Krauss, Steels: Processing, Structure, and Performance, ASM International, Materials Park, 2005.

[10] D. Klobčar, J. Tušek, B. Taljat, Thermal fatigue of materials for die-casting tooling, Mater. Sci. Eng. A 472.1 (2008) 198-207.